Regulating solvation and interface chemistry enables advanced aluminum-air battery

Chaonan Lv[#], Yuxin Zhang[#], Yixin Li*, Yuanxin Zhu, Jialin Kuang, Yougen Tang, Haiyan Wang*

Hunan Provincial Key Laboratory of Chemical Power Sources, College of Chemistry and Chemical Engineering, Central South University, Changsha, 410083, P. R. China.

Corresponding author:

*E-mail: yixinli@csu.edu.cn (Yixin Li);

*E-mail: wanghy419@csu.edu.cn (Haiyan Wang).

# Chaonan Lv and Yuxin Zhang contributed equally to this work.

Experimental Section

Electrode preparation: The aluminum alloy used in this work was purchased from Changzhou Yoteco, and its elemental composition is shown in Table S1. The aluminum alloy was mechanically polished with sandpaper, then washed with deionized water and absolute ethanol in an ultrasonic cleaner for 5 min, respectively, and then dried in a vacuum at 70 °C for 8 h to obtain the anode material. The air cathode is commercially available which is composed of a $Mn_xO_y@Ag$ catalyst, gas diffusion layer and Ni mesh current collector.

Electrolyte preparation: Potassium hydroxide was of the analytical grade from Shanghai Chemical Reagent Company of China. Methylurea (MU) and $SnCl_2$ were purchased from Macklin. By adding different molar masses of MU and $SnCl_2$ to 4 mol L^{-1} KOH solution, 3 M MU (3 mol kg^{-1}), 20 mM $SnCl_2$ (20 mol kg^{-1}) were prepared, while 4 M KOH solution was marked as blank.

Characterization: The morphology and composition of the aluminum surface were systematically investigated by using a scanning electron microscope (SEM, Nova Nano-SEM 230) and in situ optical microscope (Nikon, SMZ25). Raman spectra were collected on a Renishaw inVia spectrometer. Fourier transform infrared (FT-IR) spectra were obtained using a Bruker Vertex 70 FT-IR spectrophotometer. [1]H nuclear magnetic resonance (NMR) spectra were recorded on a 300.5 mm glass NMR tube. Samples were analyzed at 25 ± 0.1°C. Data were processed in MestReNova 11.0.2.

Electrochemical measurements: Electrochemical measurement was carried out in a conventional three-electrode cell by using a CHI760 electrochemical workstation,

which used an aluminum alloy (10 mm × 10 mm × 3 mm) as the working electrode (WE), a Hg/HgO electrode as the reference electrode (RE) and platinum as the counter electrode (CE). The potentiodynamic polarization curves were obtained from 0.5 V to 1.5 V vs. the open circuit potential (OCP). The electrochemical impedance spectroscopy (EIS) experiments were performed at the OCP in the frequency from 100 kHz to 0.01 Hz with 5 mV amplitude. The electrochemical windows of the different electrolytes were obtained by linear sweep voltammetry (LSV) at 1 mV s^{-1} in the three-electrode system.

Aluminum–air full battery tests: The aluminum-air batteries were composed of an aluminum plate anode, electrolyte and two cathode films with a Mn_xO_y@Ag catalyst. To obtain discharge curves, the electrolytes (100 mL) were put in sealed bottles and kept flowing. The mass-specific capacity of the full battery was calculated by dividing the mass difference of the aluminum anode before and after galvanostatic discharge.

Electric field simulation: A simplified 2D model was established to simulate the electric field distribution at the anode/electrolyte interface based on COMSOL Multiphysics software. In this model, both the length and height of the electrode are 500.0 μm. The surface deep pits of aluminum in blank and hybrid electrolytes in this simulation are based on the in situ optical microscope observation.
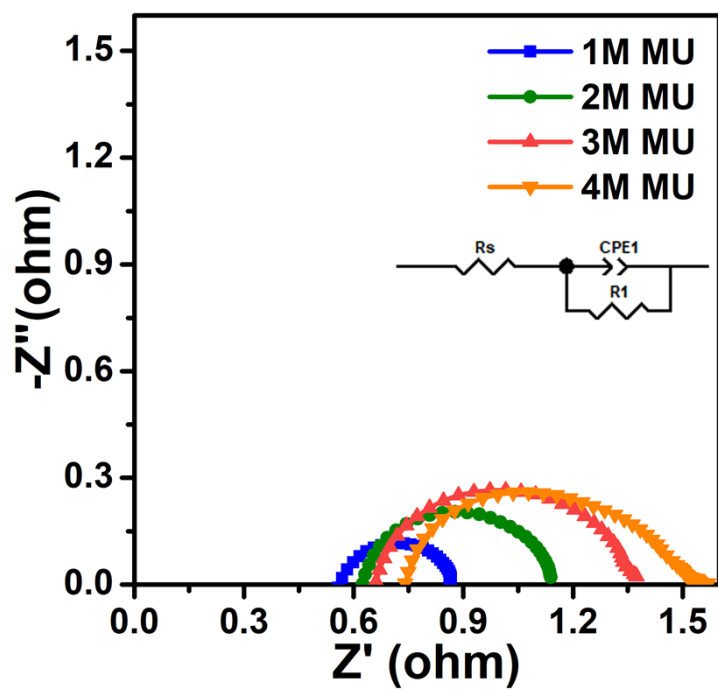
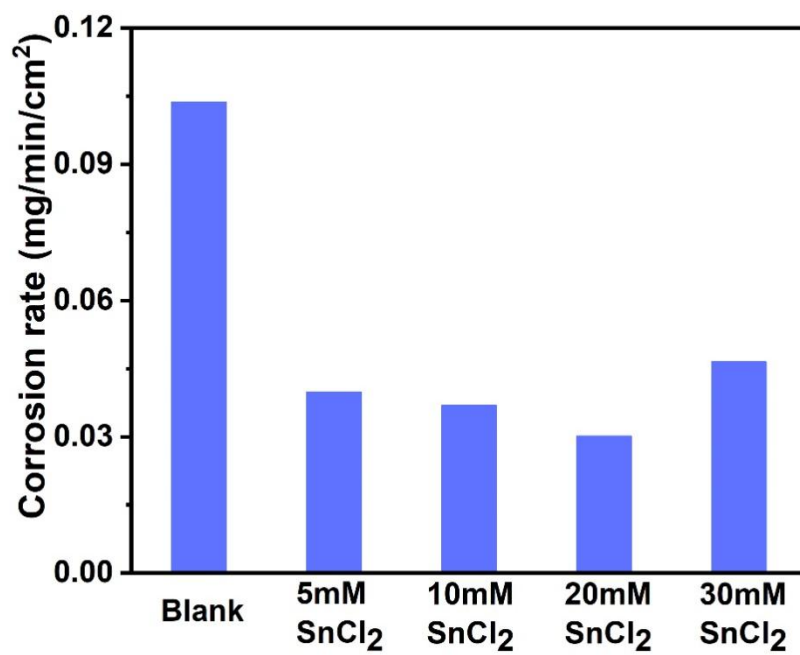**Fig. S1.** EIS spectra with various MU content.

Fig. S2. Corrosion rate of different electrolytes that contain SnCl$_2$
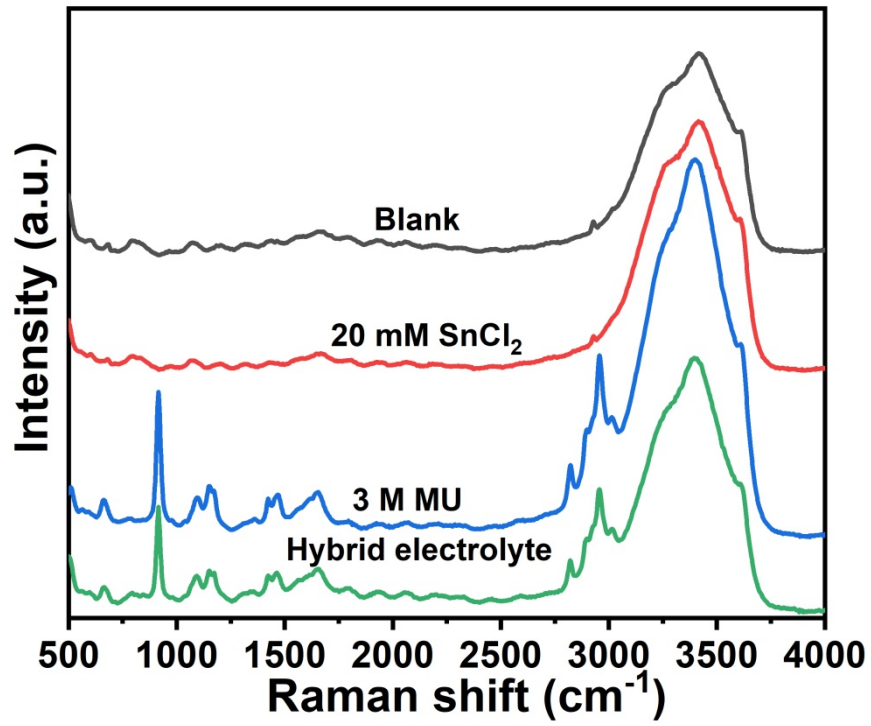
Fig. S3. Raman spectra of different electrolytes.
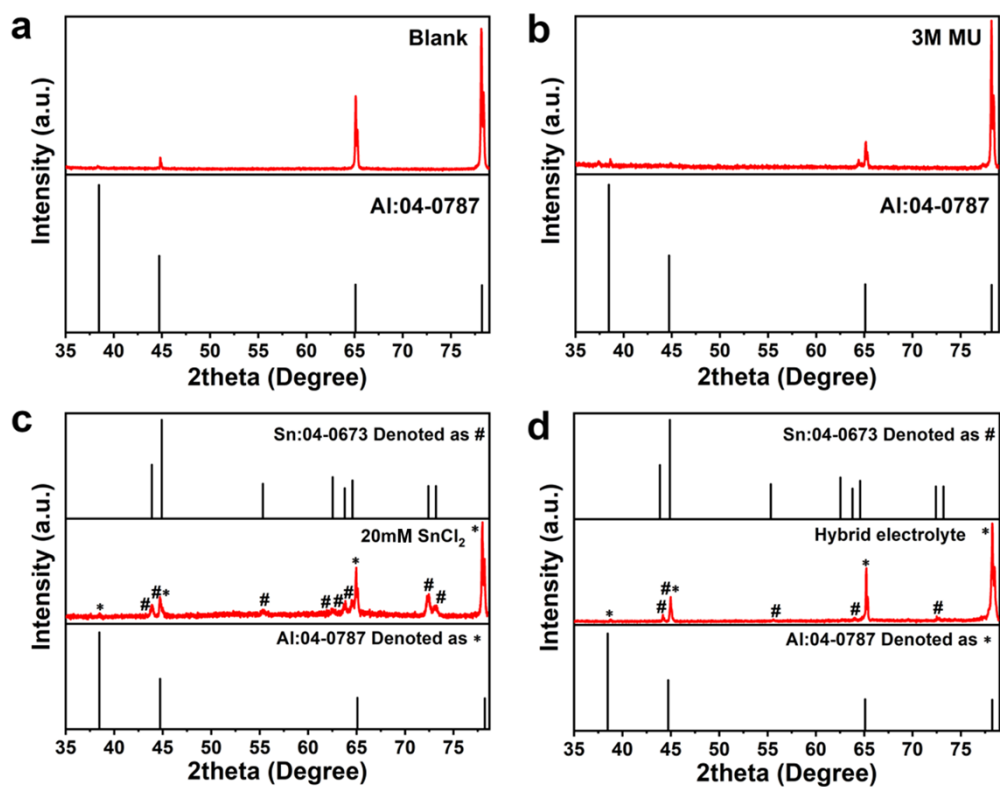
Fig. S4. XRD patterns of aluminum anode after immersing in (a) blank electrolyte, (b) 3 M MU, (c) 20 mM $SnCl_2$ and (d) hybrid electrolyte for 3 h.
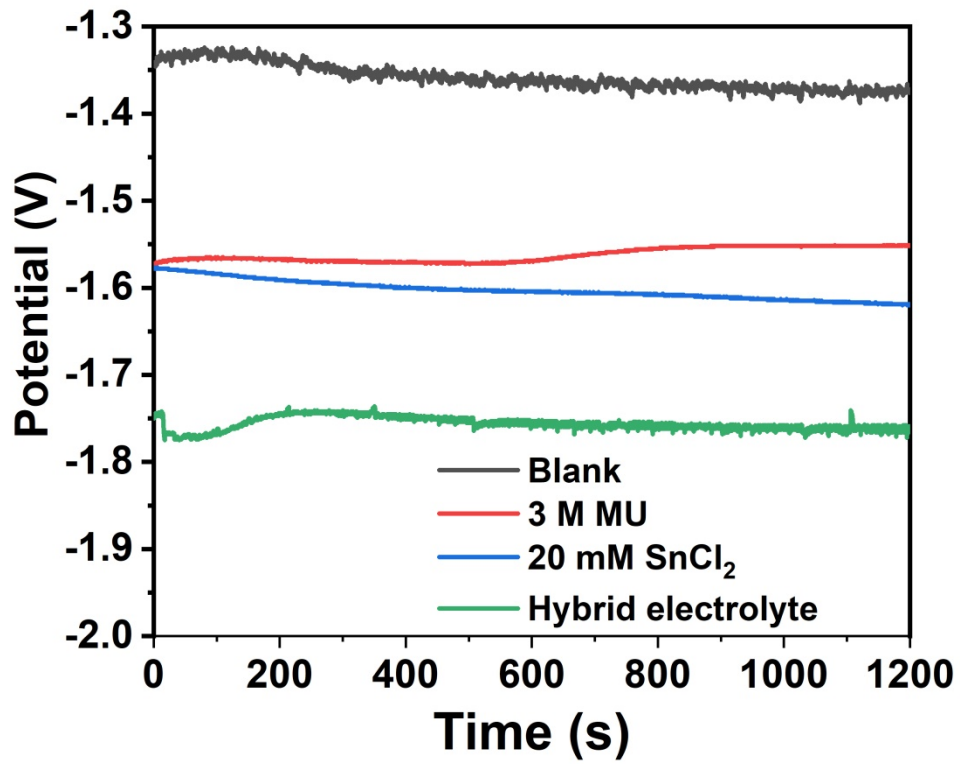
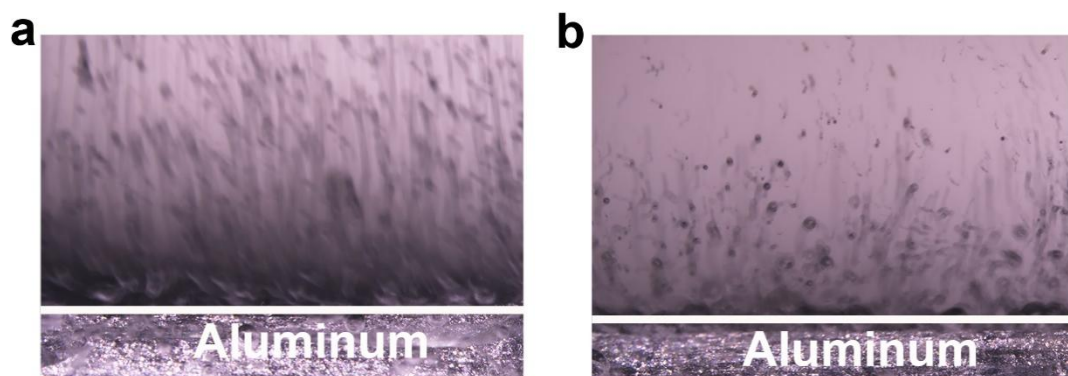**Fig. S5.** Open circuit potentials of cells with different electrolytes.

Fig. S6. In-situ optical microscope images of aluminum anode surfaces in (a) 3 M MU and (b) 20 mM SnCl$_2$.
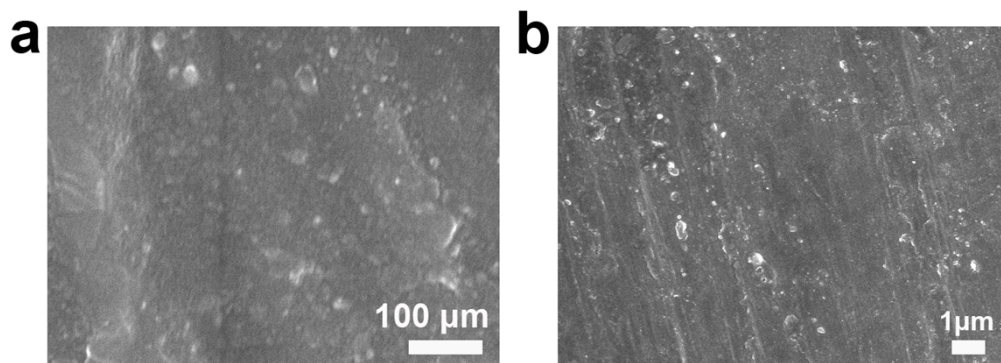
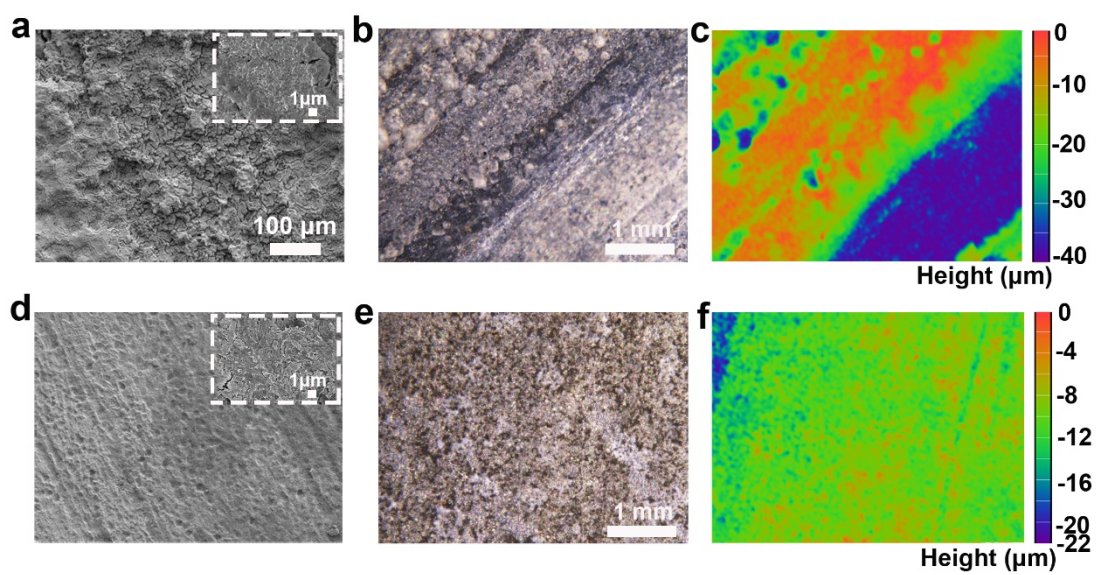**Fig. S7.** SEM images of pristine aluminum anode.

Fig. S8. SEM and in-situ optical microscope images of aluminum anode after immersing in (a)-(c) 3 M MU and (d)-(f) 20 mM SnCl$_2$ for 3 h.
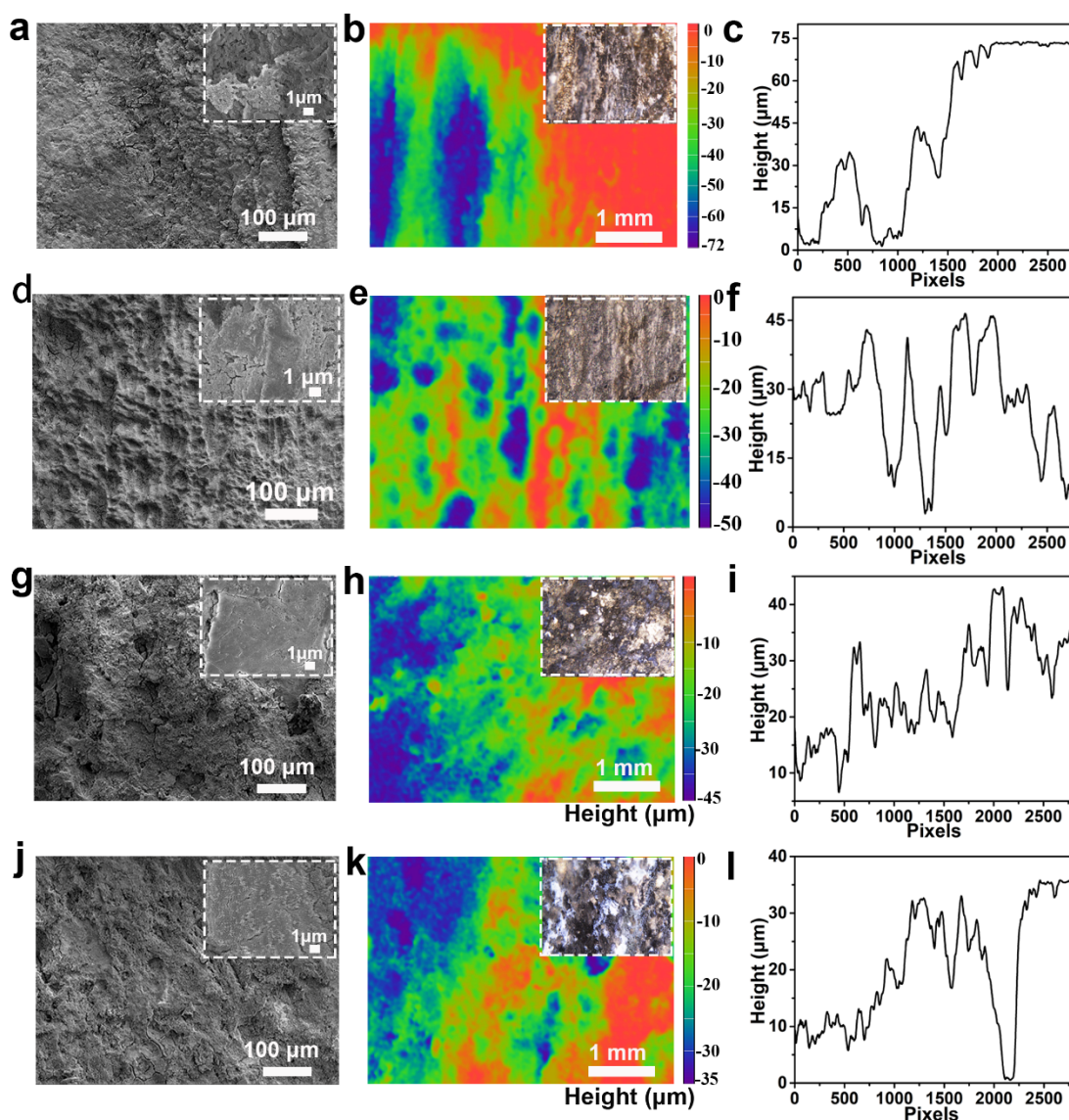
Fig. S9. SEM and in-situ optical microscope of aluminum anode surface in the electrolytes of (a)-(c) blank, (d)-(f) 3 M MU, (g)-(i) 20 mM SnCl$_2$ and (j)-(l) hybrid electrolytes after 6 h galvanostatic discharge at 50 mA cm^{-2}.

Fig. S9a shows the SEM image of aluminum surface after galvanostatic discharge at 50 mA cm^{-2} for 6 h in the blank electrolyte. It can be seen that there are numerous cracks on the surface and the corrosion depth even reaches 72 μm (Fig. S9b-c), which means that the aluminum anode is severely corroded during discharging. And this uneven structure is also observed on the aluminum anode surface with 3 M MU (Fig.

S9d-f). Aluminum anode surface becomes relatively flat when the electrolyte contains 20 mM $SnCl_2$ and the in-situ optical microscope shows the corrosion depth is 45 μm (Fig. S9g-i). As for hybrid electrolyte, the aluminum anode surface is smoother than any others. In addition, an in-situ optical microscope also confirmed this result and the maximum corrosion depth is 35 μm, revealing the uniform stripping of aluminum ions. Furthermore, XRD test results show that the in-situ generated Sn protective layer on the aluminum anode surface in electrolytes containing $SnCl_2$ remained after galvanostatic discharge for 6 h (Fig. S10). The above-mentioned results are in agreement with the corrosion properties in Fig. 3. Therefore, we can deduce that the presence of MU and $SnCl_2$ in electrolytes can also inhibit the self-corrosion and lead to uniform stripping of aluminum anode during galvanostatic discharge.
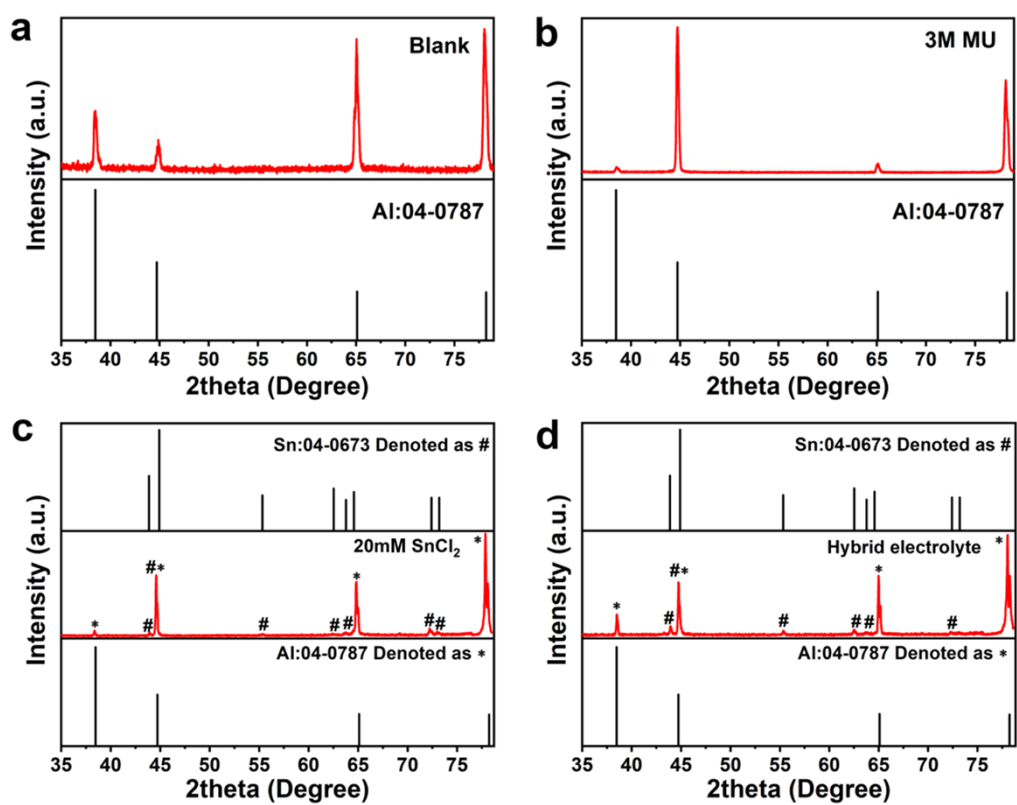
Fig. S10. XRD patterns of aluminum anode surface in (a) blank electrolyte, (b) 3 M MU, (c) 20 mM $SnCl_2$ and (d) hybrid electrolyte after galvanostatic discharge for 6 h.
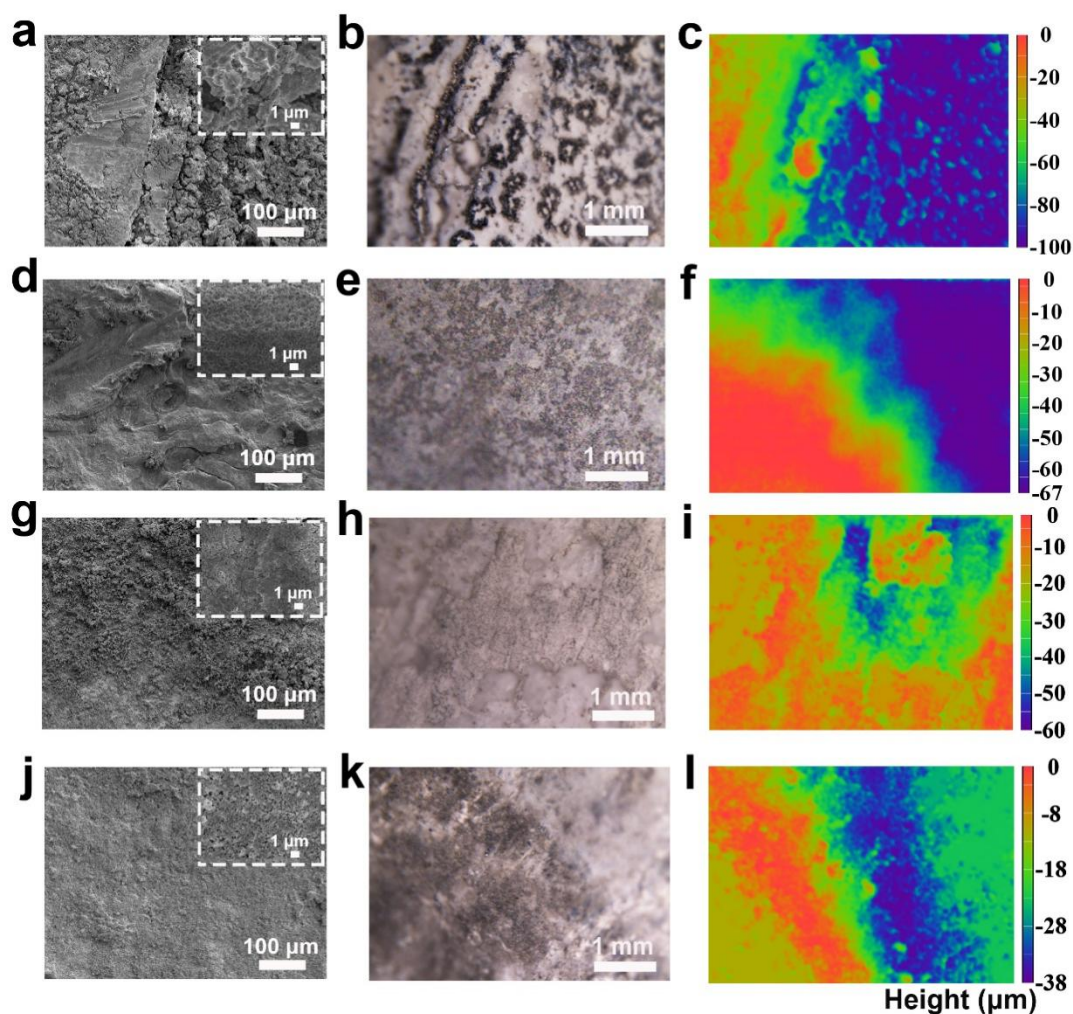
Fig. S11. SEM and in-situ optical microscope images of aluminum anode in (a)-(c) blank, (d)-(f) 3 M MU, (g)-(i) 20 mM SnCl$_2$ and (j-l) hybrid electrolyte after galvanostatic discharge.

There are many gullies and cracks on the aluminum anode surface in the blank electrolyte, indicating that aluminum anode suffers from serious self-corrosion and uneven aluminum ion stripping. However, the surface with hybrid electrolyte is much smoother than the blank one, which further confirms that the addition of MU and SnCl$_2$ successfully suppresses aluminum anode corrosion.
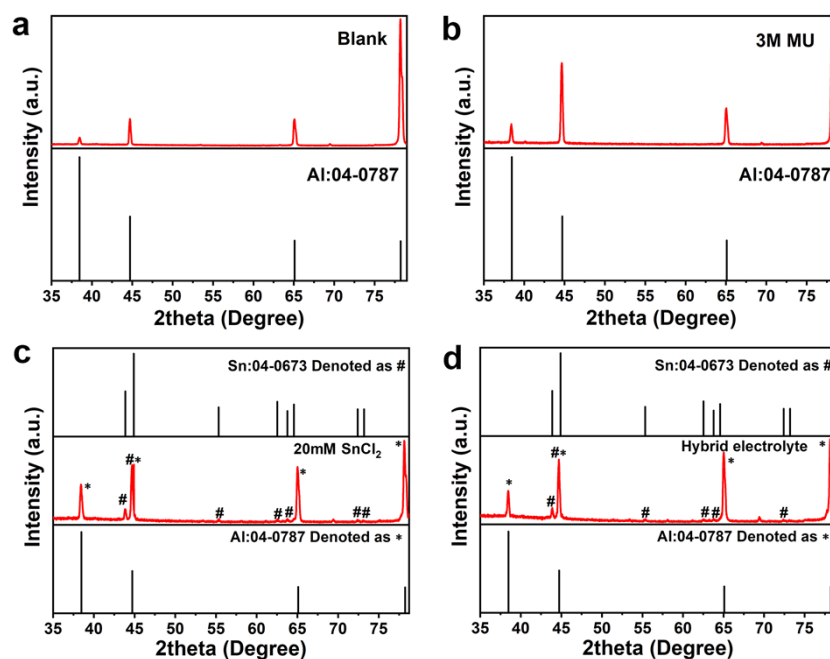
Fig. S12. XRD patterns of aluminum anode surface in (a) blank electrolyte, (b) 3 M MU, (c) 20 mM $SnCl_2$ and (d) hybrid electrolyte after galvanostatic discharge.

The element Sn can be found on the aluminum anode surface in 20 mM $SnCl_2$ and hybrid electrolyte after galvanostatic discharge, indicating that the Sn protective layer is always present on the surface of aluminum anode during the discharge process.

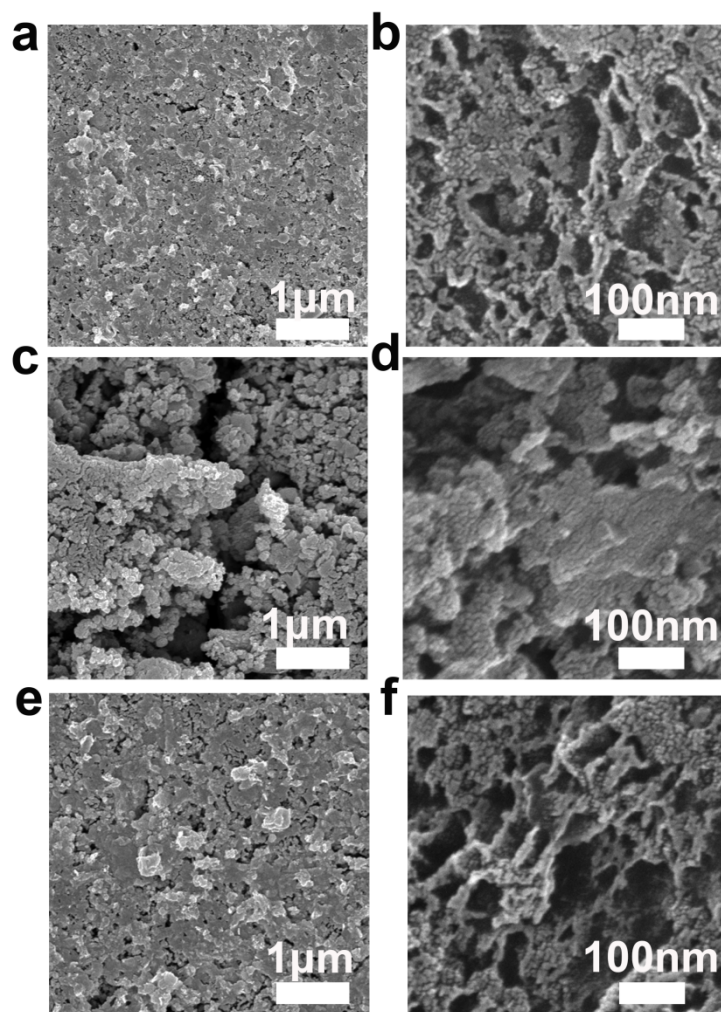**Fig. S13.** SEM images of positive electrocatalyst. (a)-(b) pristine electrocatalyst material, (c)-(d) electrocatalyst after galvanostatic discharge in blank electrolyte, (e)-(f) electrocatalyst after galvanostatic discharge in hybrid electrolyte.
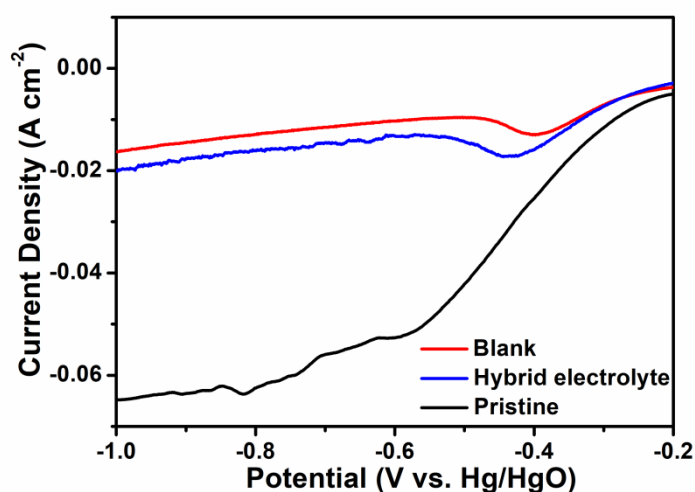
Fig. S14. LSV curves (1600 rpm) of electrocatalysts in different electrolytes after galvanostatic discharge in 0.1 M KOH solution.

Fig. S13 shows that the pristine electrocatalyst structure is hierarchical, which facilitates the diffusion of oxygen inside the electrocatalyst. After galvanostatic discharge, the electrocatalyst structure was severely damaged in the blank electrolyte but maintained well in the hybrid electrolyte, indicating the hybrid electrolyte protects the electrocatalyst to some extent. In addition, the ORR also reveals that catalyst performance significantly decline after discharge in the blank electrolyte (Fig. S14).

Table S1 Chemical compositions of Al alloy (wt %)

Mg	Ga	Sn	Zn	Fe	Cu	Si	Al
0.024	0.011	0.010	0.004	≤0.009	≤0.001	≤0.001	Remainder

Table S2 Fitting results of the Nyquist plots using the equivalent circuit.

Electrolyte	R_S (Ω cm^{-2})	CPE		R_1 (Ω cm^{-2})
		Y_0 (Ss^n cm^{-2})	n	
1M MU	0.581	5.8×10^{-4}	0.888	0.289
2 M MU	0.629	5.8×10^{-4}	0.879	0.517
3 M MU	0.649	6.5×10^{-4}	0.822	0.728
4M MU	0.671	2.0×10^{-3}	0.698	0.862

Table S3 Fitting results of the Nyquist plots using the equivalent circuit.

Electrolyte	$R_S(\Omega\ cm^{-2})$	CPE		$R_1(\Omega\ cm^{-2})$
		$Y_0\ (Ss^n\ cm^{-2})$	n	
Blank	0.617	2.9×10^{-4}	0.956	0.290
3 M MU	0.649	6.5×10^{-4}	0.822	0.728
20 mM SnCl$_2$	0.615	4.1×10^{-4}	0.871	0.440
Hybrid electrolyte	0.662	7.4×10^{-4}	0.895	0.858

Table S4 Corrosion rate of aluminum anode in different electrolyte.

Solution	$\Delta m(mg)$	$R(mg\ cm^{-2}\ min^{-1})$	$\eta\%$
Blank	116.3	0.110	-
3 M MU	57.6	0.057	48.18
20 mM SnCl$_2$	21.4	0.021	80.91
hybrid electrolyte	12	0.011	90.9